Two-dimensional Steady Heat Conduction

Pratik M Panchal (AM22S033), Manjunath N (AM22D014)

September 11, 2022

Assignment - 1

Foundations of CFD (AM5630)

V. D. Narasimhamurthy

Department of Applied Mechanics, IIT Madras

1 Methodology

1.1 Physical description of the problem

The study aims to solve the two-dimensional steady heat conduction over the simple rectangular domain with different boundary condition, as shown in Fig. 1(a) and (b). The length (L) and height (H) of computational domain are 1and 0.5, respectively.

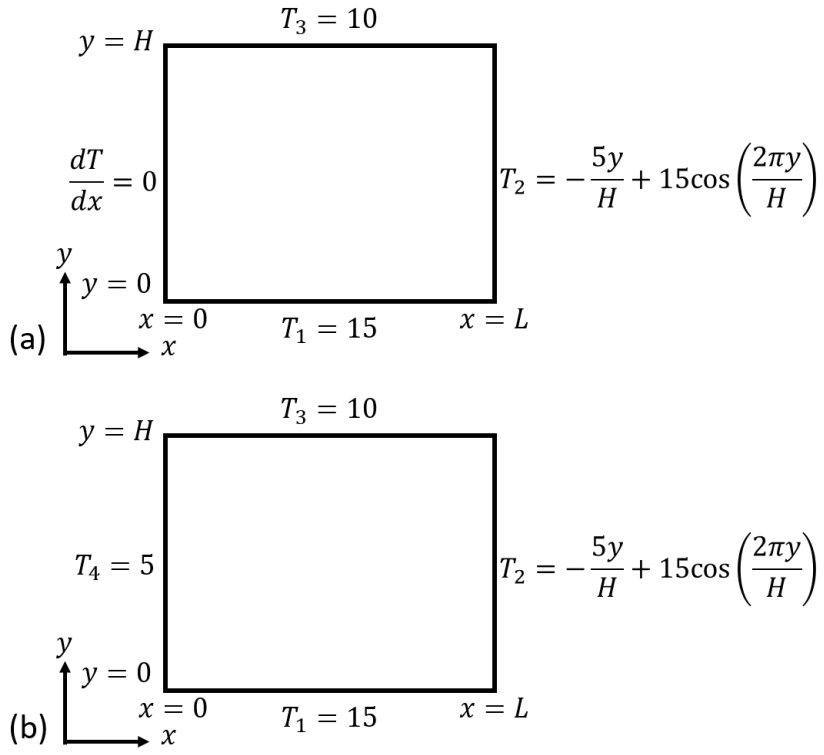

Figure 1: Computational domain for two-dimensional steady heat conduction for first problem (a) and second problem (b).

1.2 Governing Equation for heat conduction

The governing equation for the two-dimensional, steady heat conduction are as follows:

$$\frac{\partial}{\partial x}\left(k\frac{\partial T}{\partial x}\right) + \frac{\partial}{\partial y}\left(k\frac{\partial T}{\partial y}\right) + S = 0 \tag{1}$$

Here, x and y are coordinates in x and y direction, respectively. T is temperature and heat generation per unit area (S) equals to -1.5. k is thermal conductively, defined as linear function of x.

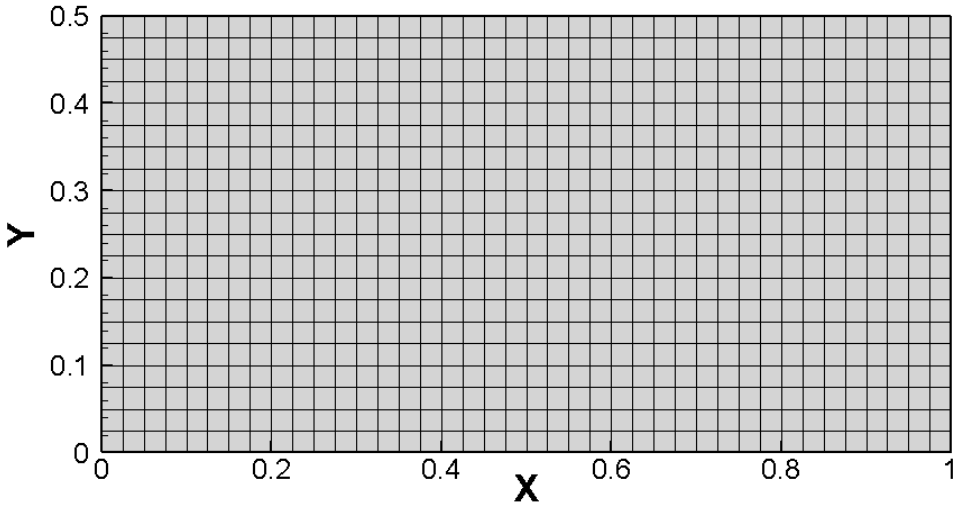

Figure 2: Computational uniform-grid ($40\,X\,20, \Delta x = \Delta y$)

$$k = 5\left(1 + 100\frac{x}{L}\right)$$

For the first problem, insulation boundary condition ($^{dT}/_{dx} = 0$) is applied on left wall. The dirichlet boundary condition is applied on top ($T_1 = 15$) and bottom ($T_3 = 10$) wall. The cosine varying temperature profile is imposed on right wall. In the second problem, only the left wall neuman boundary condition ($^{dT}/_{dx} = 0$) is changed to dirichlet ($T_4 = 5$) with keeping other boundary condition same. The mathematical description of boundary conditions for both the problems are given in Fig. 1(a) and (b).

1.3 Numerical details

The governing equations are solved using the Finite Volume Method (FVM) on a cartensian computational grid as shown in Fig. 2. The computational domain is discretized using the uniform ($\Delta x = \Delta y$) ($40\,X\,20$) as well as non-uniform ($40\,X\,20$) grids. In non-uniform grid, the mesh is streched towards left wall to make finer mesh nearer the right wall. We also compared the non-uniform mesh with uniform mesh, using 5 % and 8 % strech factor in following Sec. 2.3. The simulation is done using C++ code. The central differencing (CD) scheme (second-order) is used to discretize heat conduction. The source term is directly put in average form (equal to $\overline{S}\Delta y\Delta x$). A simple Gauss- Seidel iterative procedure is used to solve linear system of equation with Root Mean Squre (RMS) tolerance of 10^{-6}. The comparison is also carried out with keeping higher RMS tolerance equal to 10^{-4} in Sec. 2.4.

2 Results and Discussion

The present study peformed detail analysis for the first problem in subsequent sections. In the end, the results of first problem is compared with change in one of neuman boundary condition to dirichlet i.e, second problem in Sec. 2.5.

2.1 Grid Independent study

To perform the grid-independence study, it is perferable to select the most variation of governing variable i.e, temperature along particular x or y direction. In the present study, the temperature variation over a section at $y = H/2$, along x-direction is compared for different uniform-grid ($\Delta x = \Delta y$) sizes–$8\,X\,4, 20\,X\,10, 40\,X\,20$ and $50\,X\,25$ in Fig. $3(a)$. Since the selected criterion of convergence is too fine (10^{-6}) for such a simplified geometry, not much variations were found in the study. Still, there is a slightly over-prediction of temperature nearer the right wall for $8\,X\,4$ and $20\,X\,10$ grid sizes (Fig. $3(b)$). Temperature is found to be same along x-direction and as well as close to right wall for $40\,X\,20$ and $50\,X\,25$ grid. Thus, the computational uniform-grid–$40\,X\,20$ is used for the simulations.

The plot of RMS residue (10^{-6}) against the Gauss-Seidel iteration for $40\,X\,20$ –uniform grid is shown in Fig. 7. Figure 7 indicates around 789 iteration, the results is converged.

2.2 Heat flux and temperature distribution (answer of fourth question)

In Figure 4, the heat flux and temperature distribution is plotted on the computational domain ($40\,X\,20$–uniform-grid). Owing to varying boundary condition imposed at the right wall, extreme lower temperatures are present in the middle portion of right end of the domain. From the temperature distribution over the rectangular domain, it is evident that this low temperature is acting as the driving potential or reason of generated heat flux. As observed from Fig. 4, the heat flux vectors are pointing towards the low temperature (in range of -5 to -17) region in the mid right end. Also, it can be seen that the heat flux ($\dot{q_x} = -k(\partial T/\partial x)$ and $\dot{q_y} = -k(\partial T/\partial y)$) is also increasing from left to right end of the domain this can be justified as the thermal conductivity k is directly proportional to the x distance. In the left end of the computational domain, we can see from the Fig. 4, there is neligible temperature gradient due to the perfectly insulated boundary condition and low thermal conductivity values. The effect of temperature disparity between the upper and lower boundary (domination of high temperature, $T_1 = 15$ and $T_3 = 10$) can be easily identified from the regions of lower x values. The higher temperature at lower boundary dominates in the generation of heat flux in those

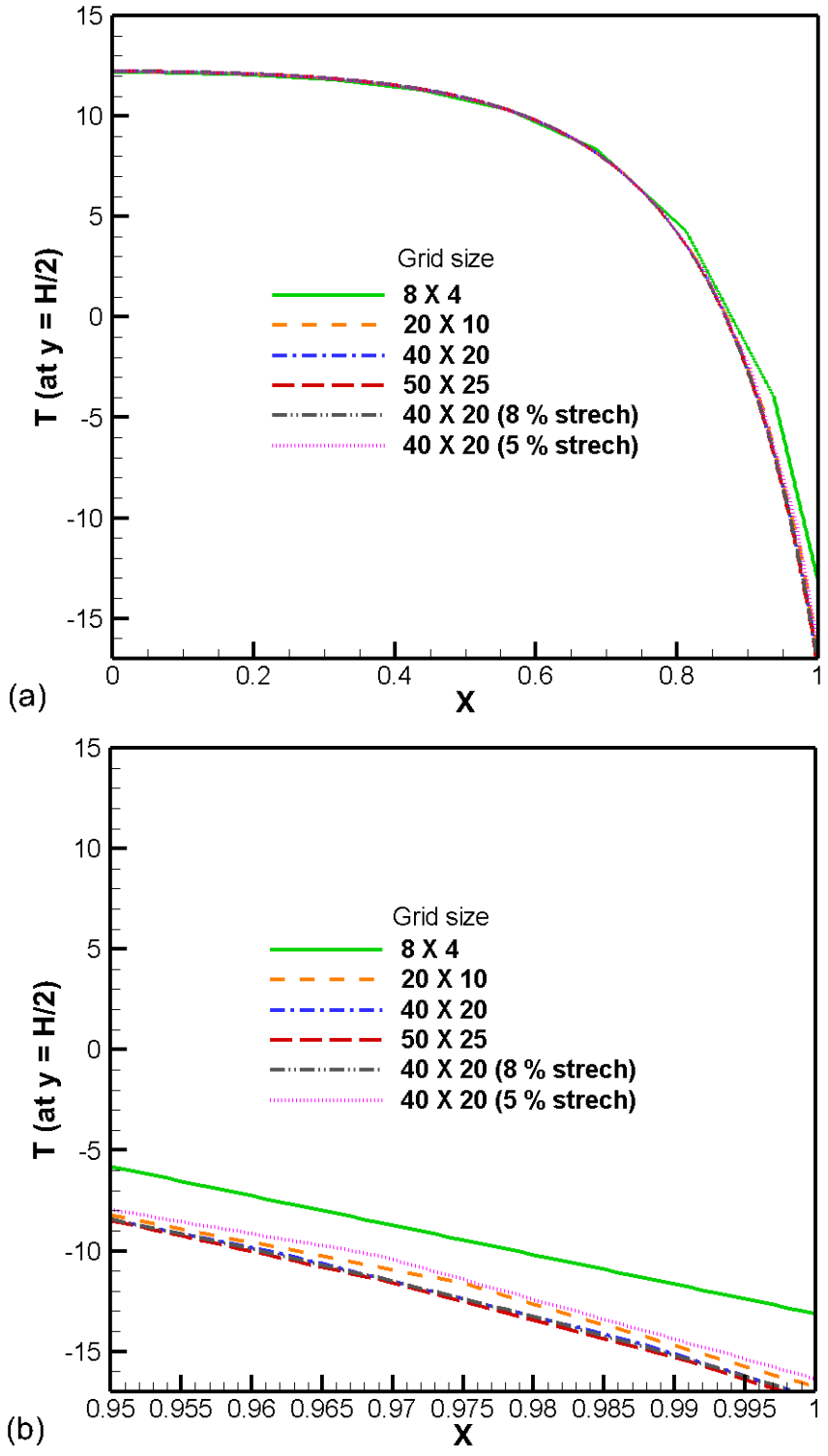

Figure 3: (a) Comparison of axial variation of the temperature at $y = H/2$ for different uniform-grid ($\Delta x = \Delta y$) sizes–$8\,X\,4, 20\,X\,10, 40\,X\,20$ and $50\,X\,25$, and non-uniform grid with 5 % and 8 % strech factor (b) enlarge region of tempeature distribution nearer to right wall.

regions.

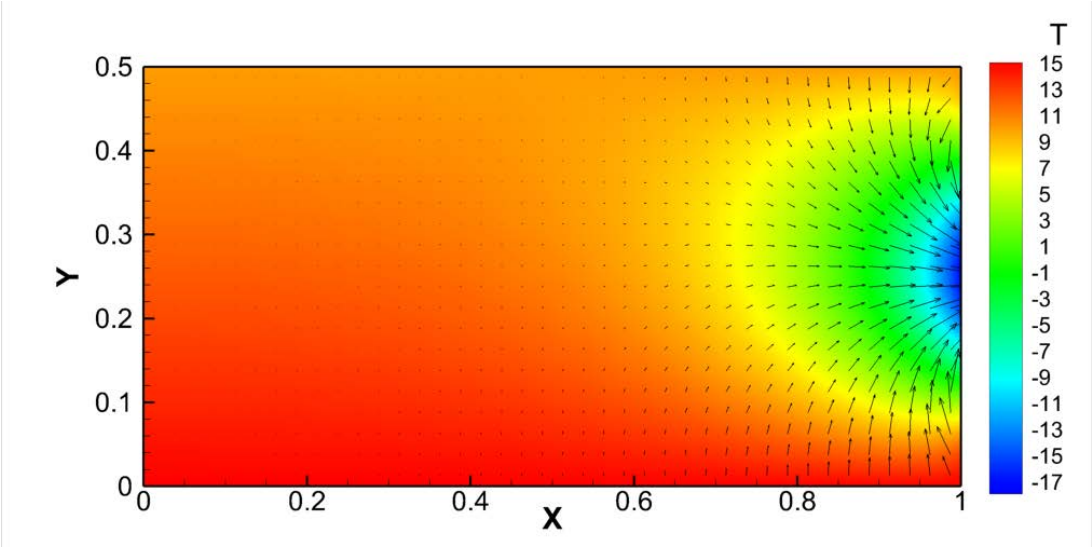

Figure 4: Temperature contour and heat flux vectors for $40\,X\,20$–uniform-grid

2.3 Comparison with non-uniform (finer) mesh (answer of first question)

From the grid independent study, it is found that $40\,X\,20$–computational uniform-grid is sufficient for the simulation. The results indicated in Fig. 4 represent a higher temperature gradient nearer to the right wall. Hence, the selected $(40\,X\,20)$ mesh is streched with two different–5 % and 8 % strech factor and compared with that of same uniform mesh in Fig. $3(a)$. The stretch factor provide more refinement in the areas of high gradient or region of importance, without increasing the computational cost. While creating the non-uniform mesh, the chances of generation of spaghetti cells are avoided by choosing the optimum stretch factor values (maintaining aspect ratio < 10).

Figure $3(b)$ represent that non-uniform mesh with 5 % strech factor is a slightly over-predicted the temperature nearer the right wall compared to the uniform mesh $(40\,X\,20)$. While, the temperature distribution of the non-uniform mesh with 8 % strech factor and uniform mesh $(40\,X\,20)$ are found to be same along x-direction and as well as close to right wall. Therefore, $40\,X\,20$– non-uniform mesh with 8 % strech factor is perferable compare to same size of uniform mesh. Here, we also plotted the temperature contours and heat flux vectors for non-uniform mesh with 5 % and 8 % strech factor in Fig. $5(a)$ and (b), respectively. As per Fig. $5(a)$ and (b), temperature contours for both type of non-uniform mesh (5 % and 8 % strech factor) are almost remains same with that of uniform-grid (Fig. 4). The density

of heat flux vectors are increasing as we proceed towards the wall, which is due to finer mesh nearer the right wall and same low heat flux vectors are observed close to left wall compared to uniform-grid case (Fig. 4).

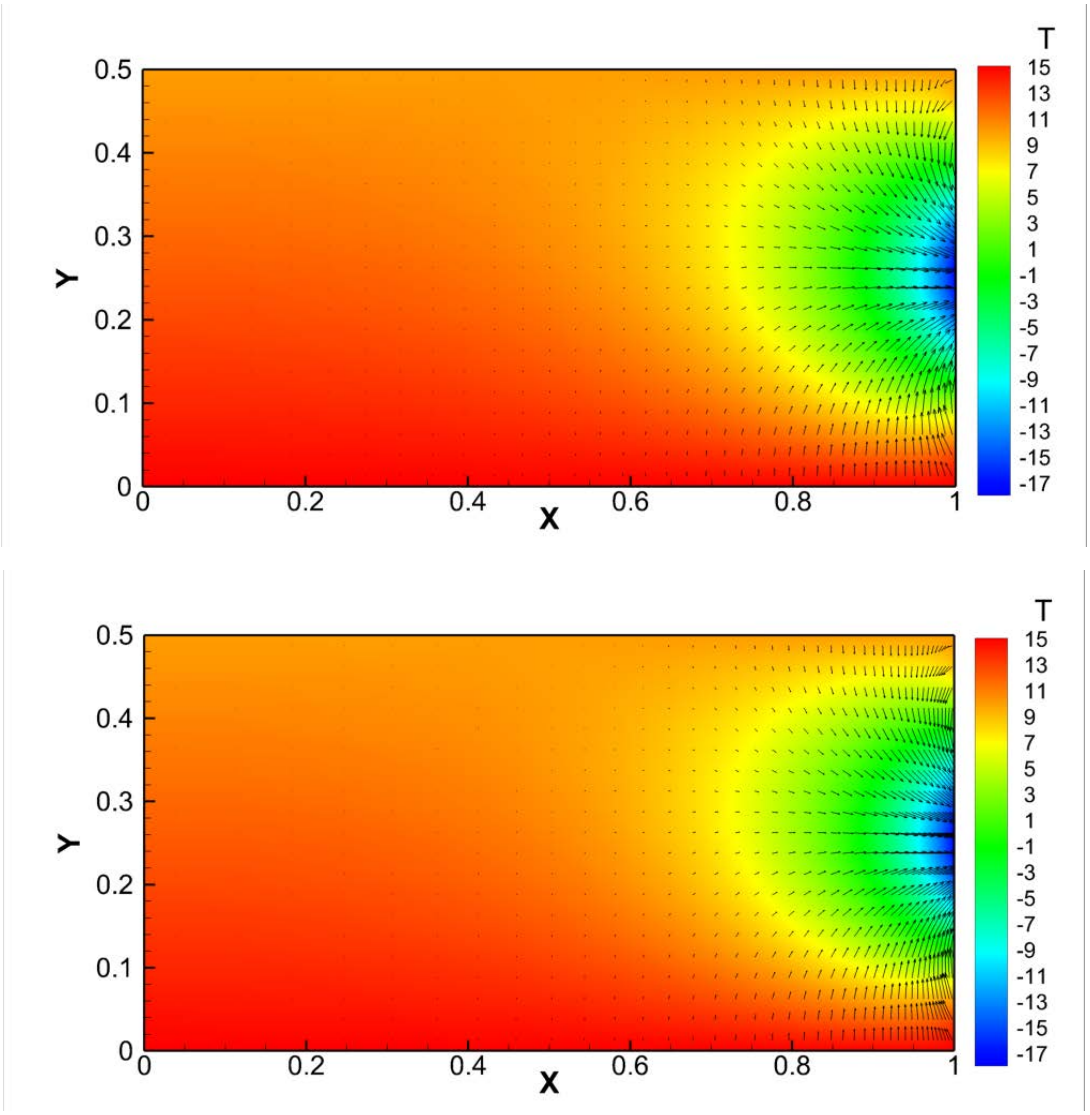

Figure 5: Temperature contour and heat flux vectors for $40\,X\,20$–non-uniform-grid with 5 % strech factor in (a), and 8 % strech factor in (b)

2.4 Effect of different convergence criterion (answer of second question)

In previous sections, numerical simulation of two-dimensional steady heat conduction (using uniform mesh–$40\,X\,20$)) is perfomed using RMS tolerance of 10^{-6}. Furthermore, to analyse

the effect of convergence criterion on results, we took another higher RMS tolerance value of 10^{-4}. In Figure 6(a), we compared the temperature variation over a section at $y = H/2$, along x-direction for two different RMS tolerance value of 10^{-4} and 10^{-6}. It is observed from the figure that the temperature distribution along x-direction for both RMS tolerance values are almost same. However, around $x = 0$ to $x = 0.3$ (in zoom section of Fig. 6(a)), temperature is under-predicted for RMS tolerance value of 10^{-4}compared to 10^{-6}. The number of iteration required to converge is obvious higher in case of 10^{-6}– RMS tolerance compared to 10^{-4}, as illustracted in Fig. 6(b). Thus, considering previous statement, we have taken convergence criterion equal to 10^{-6} for simulation.

2.5 Effect of change in neumann to dirichlet boundary condition (answer of third question)

As discussed the boundary conditions for the second problem (Fig. 1(b)) in Subsec. 1.2, we considered left wall temperature (dirichlet boundary condition ($T_4 = 5$)) equal to 5. We analysed the temperature distribution, heat flux and axial variation of temperature at $y = H/2$. It can be seen in Fig. 7 that the temperature distribution (lower value in range of -5 to -17) in mid-right end portion of geometry remains same that of previous one (Fig. 4). The nature of the heat flux vectors are also the same, pointing towards the low temperature (in range of -5 to -17) region in the mid right end, as observed from Fig. 7. The value of heat flux ($\dot{q_x} = -k(\partial T/\partial x)$ and $\dot{q_y} = -k(\partial T/\partial y)$) is also increasing from left to right end of the domain, which can be justified as the thermal conductivity k is linearly varying with the x-distance. But on the left wall, the application of constant temperature ($T_4 = 5$) instead of insulation, induced the low temperature gradient (zoom section in Fig. 7) from top and bottom wall. This observation is clearly reflected in form of heat flux vector in the zoom section of Fig. 7. The low thermal conductivity at left wall can be reason behind the low temperature gradient.

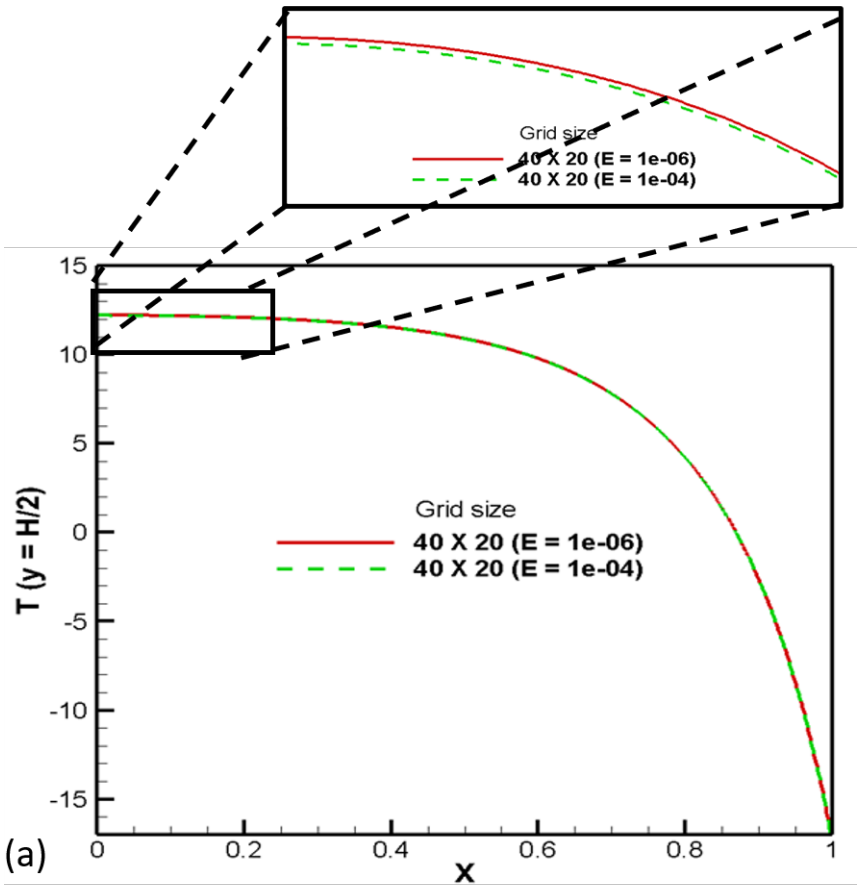

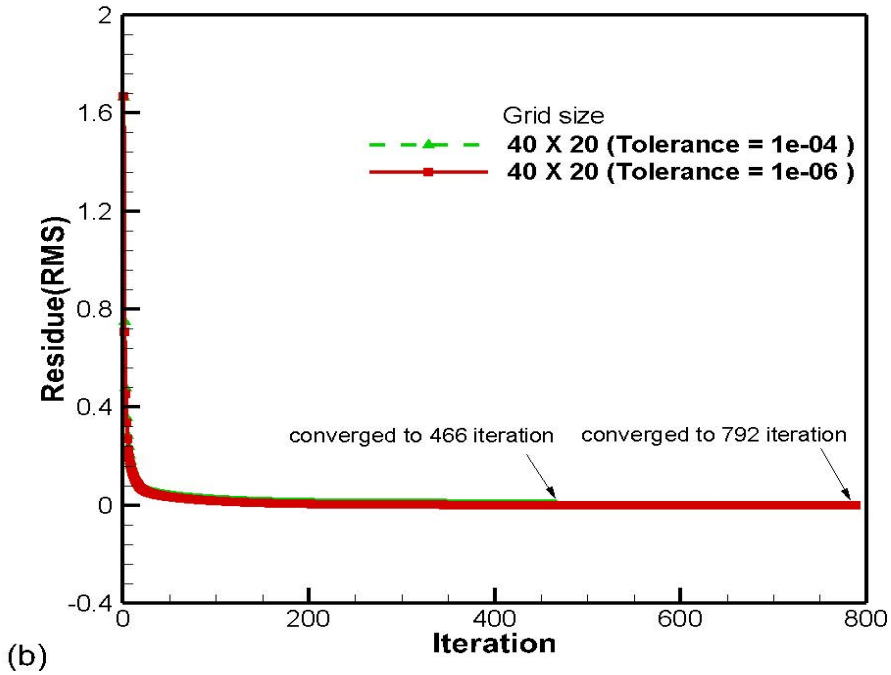

Figure 6: (a) Comparison of axial variation of the temperature at $y = H/2$ for using different convergence criterion (10^{-4} and 10^{-6}) with zoomed section from $x = 0$ to $x = 0.3$, (b) plot of RMS residue against number of interation for both 10^{-4} and 10^{-6}– convergence criterion.

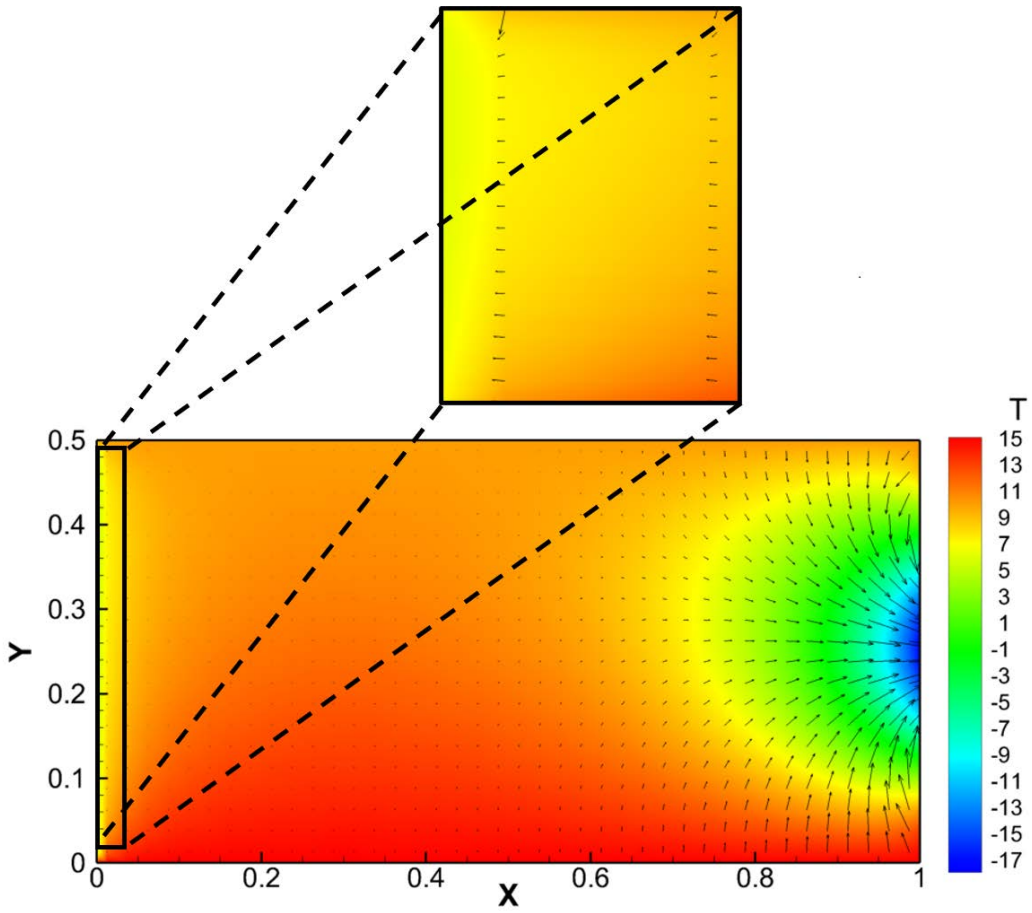

Figure 7: Temperature contour and heat flux vectors for change in neumann to dirichlet boundary condition cosidering $40\,X\,20$–uniform-grid